Available online at www.sciencedirect.com
SCIENCE DIRECT®
Journal of Solid State Chemistry 177 (2004) 936–945
JOURNAL OF SOLID STATE CHEMISTRY
http://elsevier.com/locate/jssc

Static atomic displacements of Sn in disordered NiAs/Ni_2In type HT-$Ni_{1+\delta}Sn$

A. Leineweber,[a,*] O. Oeckler,[b] and U. Zachwieja[c]

[a] *Max-Planck-Institut für Metallforschung, Heisenbergstraße 3, 70569 Stuttgart, Germany*
[b] *Max-Planck-Institut für Festkörperforschung, Heisenbergstraße 1, 70569 Stuttgart, Germany*
[c] *Lehrstuhl Anorganische Chemie I, Fachbereich Chemie der Universität, 44221 Dortmund, Germany*

Received 31 July 2003; received in revised form 22 September 2003; accepted 24 September 2003

Abstract

The crystal structures of the intermediate solid solution HT (high temperature) $Ni_{1+\delta}Sn$ with $\delta = 0.28$, 0.52 and 0.61 (refined Ni contents) have been analyzed in detail by X-ray diffraction on single crystals. The previously reported basic atomic arrangement, i.e., a NiAs/Ni_2In structure type ($P6_3/mmc$, Ni(1) on 2*a*, 0 0 0, Ni(2) with an occupancy δ on 2*d*, $\frac{2}{3}\frac{1}{3}\frac{1}{4}$, and Sn on 2*c*, $\frac{1}{3}\frac{2}{3}\frac{1}{4}$), is confirmed. However, strong anisotropic atomic displacements occur for Sn within the $a-b$ plane of the hexagonal unit cell, which require a Gram-Charlier expansion of the probability density function of Sn in order to obtain a good fit to the diffraction data. Direction, magnitude and the concentration dependence of the displacements can be interpreted in terms of the geometrical requirements of the different local atomic configurations in the planes $z = \pm 1/4$, so that the displacements can be identified as static ones.

Keywords: Disorder; Static displacements; Local atomic arrangements; Crystal structure; X-ray diffraction; Nickel–tin alloys; Non-stoichiometric phases; Intermetalics

1. Introduction

If disorder is present within a crystal structure, the occupation of atomic sites differs from unit cell to unit cell. Depending on the individual local arrangement of atoms, relaxation relative to the average atomic coordinates may occur, leading to the so-called *static displacements* [1]. Diffuse scattering provides considerable information about atomic arrangements in partially disordered crystal structures, e.g., possible short-range order and the relation between occupation of certain sites and the associated static displacements in the environment. To obtain all this information, the scattered intensity distribution over the entire reciprocal space or at least considerable parts have to be measured quantitatively.

However, valuable information can also be obtained from an analysis of the Bragg reflection intensities which are easier (compared to diffuse scattering) to measure accurately and to evaluate quantitatively on small single crystals or on powder samples. The Bragg intensities contain the space-averaged scattering density in the unit cell. For X-ray experiments this is basically the electron density, which is the convolution of the so-called probability density functions (pdfs) [2] of the different atoms with the electron densities of the single rigid atoms. The pdf itself is a convolution of a contribution from thermal vibrations and that of the above mentioned static displacements. Whereas the magnitude of static displacements should not vary strongly with changing temperature (as long as the responsible disorder remains the same) the atomic displacements due to thermal vibrations increase with temperature in a characteristic manner. In other cases the static displacement may be large compared to the vibration contributions, so their identification may also be possible without temperature dependent data.

Many theoretical and experimental studies of static atomic displacements on the basis of the evaluation of Bragg reflection intensities have been conducted for simple substitutional and interstitial solid solutions

*Corresponding author. Fax: +49-711-689-3312.
E-mail address: a.leineweber@mf.mpg.de (A. Leineweber).

0022-4596/$ - see front matter © 2003 Elsevier Inc. All rights reserved.
doi:10.1016/j.jssc.2003.09.033

based on an FCC or BCC type arrangement of metal atoms. A couple of examples have been cited in Ref. [1]. A more complex example of static atomic displacements has been analyzed for Ni rich $LaNi_5$ ($CaCu_5$ type, $P6/mmm$) [3]. A higher Ni content than $LaNi_5$ is achieved by a partial replacement of La atoms by Ni_2 dumbbells oriented parallel [001] which leads to the formula $La_{1-s}Ni_{5+2s}$. The Ni_2 dumbbells cause large static displacements of the Ni atoms surrounding these dumbbells. These displacements are well visible in corresponding electron density plots.

During studies on the order–disorder phase transitions in alloys of the composition $Ni_{1+\delta}Sn$ [4–6] of NiAs/Ni_2In structure the question about the presence and magnitude of static displacements in the disordered high-temperature (HT) phase arose. $Ni_{1+\delta}Sn$ alloys of NiAs/Ni_2In structure exist in a homogeneity range around 40 at% Sn ('Ni_3Sn_2'); specimen have yet been reported from the range $0.35<\delta<0.67$ [7]. The crystal structure of HT-$Ni_{1+\delta}Sn$ is based on a NiAs type arrangement Ni(1)Sn (axial ratio $c/a\approx1.26$). Additional Ni(2) atoms occupy partially (with an occupancy of δ) the trigonal-bipyramidal sites formed by five Sn atoms, so that the overall composition Ni(1)Ni(2)$_\delta$Sn results. The resulting 'conventional' crystallographic description of HT-$Ni_{1+\delta}Sn$ in terms of fractional coordinates and their occupancies by the different atoms is listed in Table 1.

HT-$Ni_{1+\delta}Sn$ transforms by reversible order–disorder phase transitions into different low-temperature phases labelled LT, LT′ and LT″, having all lower (orthorhombic) symmetry than the HT-phase, caused by occupational long-range ordering of Ni(2). The occurrence of one of the three different low-temperature phases is determined by the composition. LT-$Ni_{1+\delta}Sn$ has been observed for $0.45\leqslant\delta\leqslant0.50$ [5]. It forms a commensurate superstructure with unit cell parameters of $a_{LT}\approx2a_{HT}, b_{LT}\approx3^{1/2}b_{HT}, c_{LT}\approx c_{HT}$ and orthorhombic $Pbnm$ symmetry (the non-standard setting of $Pnma$ was chosen in order to keep c_{LT} parallel c_{HT}). It leads to a 1:1 differentiation of the Ni(2) sites, of whom one is fully occupied and one is empty for the ideal composition $Ni_{1.50}Sn$ ("Ni_3Sn_2") [8]. The occupational ordering is accompanied by strong displacements of the atoms, especially for Sn within the $a-b$ plane. With respect to the composition range of the LT-phase, the LT′- and LT″-phases were found to occur at lower and higher Ni(2) contents, respectively. LT′ and LT″ show incommensurate ordering patterns of Ni(2) which are closely related to the structure of the LT-phase ([4, 5], and A. Leineweber, *unpublished*).

One may be tempted to calculate interatomic distances from the conventionally formulated crystal structure of HT-$Ni_{1+\delta}Sn$ as given in Table 1, i.e., from the fractional coordinates and the unit-cell parameters. Then, the *equatorial* distance between Ni(2) and Sn within the trigonal-bipyramids $Ni(2)Sn_5$ would be $d(Ni(2)\cdots Sn)_{eq}=a_{HT}/3^{1/2}$, whereas the *axial* distance would be $d(Ni(2)\cdots Sn)_{ax}=c_{HT}/2$ (Fig. 1). For typical cell parameter values, a_{HT} and c_{HT} for different compositions [7], distances of $d(Ni(2)\cdots Sn)_{eq}=2.33$–$2.39$ Å and $d(Ni(2)\cdots Sn)_{ax}=2.56$–$2.61$ Å would be obtained. However, for virtually completely ordered (i.e., no corruption of the distances due to local static displacements is possible) LT-$Ni_{1.50}Sn$ $d(Ni(2)\cdots Sn)_{eq}=2.50$–$2.58$ Å [5] was observed. The shortest reliable distance $d(Ni\cdots Sn)$ in literature (according to

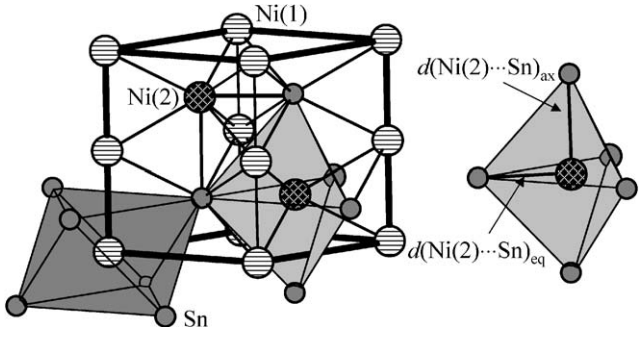

Fig. 1. Unit cell for an idealized Ni_2In/NiAs type structure with additional Sn atoms to show the octahedral coordination of Ni(1) and the trigonal-bipyramidal coordination of Ni(2) by Sn atoms, respectively. The bonds inside the indicated polyhedra are not shown. A separate trigonal-bipyramid $Ni(2)Sn_5$ is shown with the indicated axial (ax) and equatorial (eq) distances Ni(2)···Sn.

Table 1
'Conventional' description of Ni_2In/NiAs type HT-$Ni_{1+\delta}Sn$, cell parameters $a_{HT}=4.04$–4.15 Å, $c_{HT}=5.12-5.21$ Å [7], $c_{HT}/a_{HT}\approx1.26$ (see Fig. 1) as well as corresponding data for the LT-phase with orthorhombic superstructure. Note the splitting of the Ni(2) and the Sn sites in the LT-phase

HT-phase, $P6_3/mmc$ with a_{HT}, c_{HT}			LT-phase (at $\delta=0.5$), $Pbnm$ with $a_{LT}\approx2a_{HT}$, $b_{LT}\approx3^{1/2}b_{HT}$, $c_{LT}\approx c_{HT}$		
Site, Wyckoff symbol	$x\,y\,z$	Occupancy	Site, Wyckoff symbol	$x\,y\,z$[a]	Occupancy
Ni(1), 2*a*	0 0 0	1	Ni(1), 8*d*	$\frac{1}{8}\,\frac{1}{4}$ 0 (0.125 0.234 0.005)	1
Ni(2), 2*d*	$\frac{2}{3}\,\frac{1}{3}\,\frac{1}{4}$	δ	Ni(2a), 4*c*	$\frac{1}{8}\,\frac{11}{12}\,\frac{1}{4}$ (0.127 0.909, $\frac{1}{4}$)	$2\delta=1$
			Vacancy ('Ni(2b)'), 4*c*	$\frac{1}{8}\,\frac{7}{12}\,\frac{3}{4}$ (−)[b]	0
Sn, 2*c*	$\frac{1}{3}\,\frac{2}{3}\,\frac{1}{4}$	1	Sn(a), 4*c*	$\frac{1}{8}\,\frac{11}{12}\,\frac{3}{4}$ (0.142 0.902 $\frac{3}{4}$)	1
			Sn(b), 4*c*	$\frac{1}{8}\,\frac{7}{12}\,\frac{1}{4}$ (0.095, 0.560, $\frac{1}{4}$)	1

[a] Ideal values from homogeneous distortion of the unit cell and refined values for LT-$Ni_{1.50}Sn$ quenched from 473 K (in brackets), cf. Ref. [5].
[b] The Ni(2*b*) site was found in Ref. [5] to be virtually vacant. Therefore, no physically sensible measured coordinates can be given.

our knowledge) is 2.43 Å in $LuNiSn_2$ [9]. This indicates, that $d(Ni(2)\cdots Sn)_{eq} = 2.33$–$2.39$ Å calculated above for the HT-phase is strikingly short. This has previously been interpreted in terms of an increase in strength of the equatorial bonds Ni(2)···Sn in the HT-phase compared to the LT-phase; even a double bond character of the equatorial bond in the HT-phase has been discussed [10]. It is, however, much more likely, that in the HT-phase the presence of Ni(2) in trigonal-bipyramids is accommodated by static displacements of Sn atoms on a local scale, away from the ideal $\frac{1}{3}\frac{2}{3}\frac{1}{4}$ coordinates. Indeed, there are hints from size-effect-type intensity transfer in the diffuse electron scattering intensity [11] that displacements of Sn may be significant in HT-$Ni_{1+\delta}Sn$. Furthermore, for another disordered NiAs/Ni_2In type alloy phase, $Fe_{1+\delta}Ge$, static displacements of Ge have been reported for two close compositions ($\delta = 0.60$ [12], 0.67 [13]) and described by a split atom model for Ge. In this way unreasonably short Fe(2)···Ge distances (similar as to the equatorial Ni(2)···Sn distances in HT-$Ni_{1+\delta}Sn$) are avoided.

In the present work the regular Bragg reflection intensities of HT-$Ni_{1+\delta}Sn$ single crystals are analyzed for a wide range of composition, in order to check for the presence of static displacements of Sn and to reveal possible concentration dependent effects.

2. Experimental

2.1. Preparation

$Ni_{1+\delta}Sn$ alloys (δ from the weighted amounts of Ni and Sn: 0.35, 0.50 and 0.63) were prepared from Ni sheets (1 mm thickness, 99.98 mass%, Goodfellow) and Sn pieces (bars, Heraeus 99.999 mass%). The batch sizes were about 3 g $Ni_{1+\delta}Sn$. The starting materials were melted by induction heating in alumina crucibles and cooled in the furnace. The reguli were sealed in quartz tubes and annealed for homogenization for 2 d at 473 K and 2 d at 1023 K followed by water quenching (the quartz tubes were crushed while being held under water so that the reguli came into direct contact with the water leading to a high cooling rate). The weight of the initial metals and the reguli were compared and no significant change was indicated for any of the three alloys. Therefore, the average compositions of the alloys could be assumed to be identical to those expected from weighting.

2.2. X-ray powder diffraction

For determination of cell parameters, parts of the reguli were ground in a mortar and mixed with Ge powder as internal standard ($a = 5.6574$ Å). Powder diffraction patterns were recorded on a Huber imaging plate Guinier camera G670 employing Cu$K\alpha$1 radiation ($\lambda = 1.54056$ Å). Reflection positions were extracted using the program CMPR [14], and those of $Ni_{1+\delta}Sn$ were corrected for those of Ge. Unit cell parameters were refined from the corrected reflection positions using the program ASIN [15].

2.3. Single crystal X-ray diffraction experiments and data reduction

Single crystals were isolated from a crushed part of the reguli under an optical microscope. The crystals corresponding to the three alloys are referred to furtheron by $Ni_{1.35}Sn$, $Ni_{1.50}Sn$ and $Ni_{1.63}Sn$, i.e., by formulas representing the average compositions of the alloys, irrespective from the compositions obtained by structure refinement. The crystals were mounted in glass capillaries. X-ray diffraction experiments on these single crystals were performed on a CAD4 diffractometer (Enraf-Nonius, Delft, NL) employing Ag$K\alpha$ radiation. A 'full sphere' of reflections was measured in each case. Details of the measurements are listed in Table 2. Data reduction was performed using tools provided by Jana2000 [16]. The intensity data were corrected for absorption starting from a measured crystal shape, which was then optimized applying the program X-Shape [17]. After averaging according to the 6/*mmm* Laue symmetry the structure refinement was performed.

2.4. Structure refinement

Structure refinements on the basis of the single crystal diffraction data were performed using Jana2000 [16]. The initial model was the 'conventional' model for the Ni_2In/NiAs type structure as given in Table 1 allowing for isotropic Gaussian atomic displacements, and a varying occupancy of Ni(2). Since this structure model gave only poor residuals, more elaborate methods had to be applied to describe the atomic displacements.

For the $Ni_{1.50}Sn$ crystal the improvement of the residual parameters upon subsequently adding groups of atomic displacement parameters is documented in Table 3. Upon adding each group of new parameters the Hamilton test is passed [18], indicating the significance of the added parameters. The final *main model* considers anisotropic Gaussian atomic displacements modified by Gram-Charlier series parameters [2] up to the orders 5 (Sn) and 4 (Ni(1)) in order to describe the non-Gaussian character of the pdfs of Sn and Ni(1). Together with the overall scale factor, an extinction parameter as well as the occupancy of Ni(2), altogether 19 parameters are refined for the *main model* (cf. Table 4).

For the $Ni_{1.35}Sn$ and $Ni_{1.63}Sn$ crystals only the addition of the 4th order Gram-Charlier parameters for Ni(1) atoms does not pass the Hamilton

Table 2
Details of data collection and the least-square refinement procedure for the structure refinement using single crystal diffraction data on HT-$Ni_{1+\delta}Sn$ of three different compositions

Diffractometer		Enraf-Nonius CAD4	
Wavelength		0.56083 Å (Ag$K\alpha$)	
Crystal size (mm^3)	$0.06 \times 0.08 \times 0.09$	$0.025 \times 0.025 \times 0.0125$	$0.015 \times 0.07 \times 0.08$
Crystal label[a]	*$Ni_{1.35}Sn$*	*$Ni_{1.50}Sn$*	*$Ni_{1.63}Sn$*
Formula of the crystal from refinement (cf. Table 3)	$Ni_{1.275(6)}Sn$	$Ni_{1.524(4)}Sn$	$Ni_{1.614(5)}Sn$
Space group type (No.)		$P6_3/mmc$ (194)	
Unit cell parameters			
a (Å)	4.0524(3)	4.103(1)	4.1373(3)
c (Å)	5.1256(2)	5.176(1)	5.2050(4)
Number of formula units per unit cell		2	
$h;k;l$		± 12; ± 12; ± 15 ('whole sphere')	
Angular range, 2θ (deg)		6–90	
Absorption correction		Gaussian integration using crystal shape	
Calc. absorption coefficient μ_{calc}	$17.3\,mm^{-1}$	$18.1\,mm^{-1}$	$18.6\,mm^{-1}$
Transmission, min/max	0.614/0.649	0.435/0.782	0.314/0.696
Internal R value after absorption correction, all reflections/$I > 3\sigma(I)$	0.0336/0.0270	0.0755/0.0386	0.0507/0.0330
Software used for least squares refinement		Jana2000 [16], refinement based on F^2	
Number of measured reflections	4626	5132	4932
with $I > 3\sigma(I)$	2930	2678	2850
Number of independent reflections, all/$I > 3\sigma(I)$)	266/179	274/179	282/170
Extinction model		Becker and Coppens type 1, Gaussian [19]	
Number of refined parameters		19	
R, all/$I > 3\sigma(I)$	0.0344/0.0142	0.0470/0.0206	0.0717/0.0205
R_w, all/$I > 3\sigma(I)$	0.0620/0.0488	0.0568/0.0482	0.0718/0.0525
Residual electron density, max/min ($e\,Å^{-3}$)	1.23/−1.45	1.60/−1.56	2.66/−1.92

The structure model is based on Table 1 as well as the *main model* as described in the text. For the results of the refinements cf. Table 4.
[a] In the course of the discussion the alloy compositions in italics are used to label the crystals. It has to be pointed out that the refined compositions are slightly away from these values (see Table 4).

Table 3
Structure refinement for the *$Ni_{1.50}Sn$* crystal: Evolution of the residuals upon increasing successively the complexity of the models for atomic displacements (nth order indicates the highest order of a Gram-Charlier series used to refine the pdf for the corresponding atom). The last line corresponds to the *main model* which was finally adopted for all three sets of single crystal data (cf. Table 3)

Structure model	R, all/$I > 3\sigma(I)$	R_w, all/$I > 3\sigma(I)$	No. of refined parameters
All atoms isotropic	0.2763/0.2410	0.5503/0.5452	6
All atoms anisotropic	0.1353/0.1071	0.2908/0.2848	9
Sn '3rd order'	0.0787/0.0563	0.1473/0.1439	10
Sn '4th order'	0.0652/0.0328	0.0907/0.0820	13
Sn '5th order'	0.0596/0.0313	0.0829/0.0762	15
Sn '5th order' + Ni(1) '4th order'	0.0470/0.0206	0.0568/0.0482	19

test. However, in order to keep the *main model* identical with that of the *$Ni_{1.50}Sn$* crystal, this situation was accepted (cf. Table 4).

Based on considerations made in Section 3, further structure refinements were performed for the *$Ni_{1.50}Sn$* crystal data employing a structure model based on Ni(1) and Ni(2) as in the *main model* as well as a *split atom model* with isotropic atomic displacements for the pdf of Sn. Details of the latter model are described there.

3. Results and discussion

3.1. Composition of the crystals

The refined occupancies of the Ni(2) sites do not exactly correspond to the values expected from the weighted amounts of Ni and Sn used to prepare the alloys (cf. Table 3). The strongest difference between balanced and refined compositions is encountered for

Table 4
HT-$Ni_{1+\delta}Sn$: Final parameters from structure refinement ('main model') using single crystal data

Alloy/crystal[a]	*Ni1.35Sn*	*Ni1.50Sn*	*Ni1.63Sn*
Ni(1) 0 0 0:			
U_{11}[b] (Å^2)	0.0092(4)	0.0092(3)	0.0095(4)
U_{33}[b] (Å^2)	0.0070(5)	0.0062(3)	0.0072(5)
D_{1111}[c] 10,000 (Å^4)	−0.004(1)	−0.0135(9)	−0.001(2)
D_{1113}[c] 10,000 (Å^4)	0.0002(4)	−0.0067(5)	−0.0002(5)
D_{1133}[c] 10,000 (Å^4)	0.0001(2)	−0.0017(2)	−0.0002(3)
D_{3333}[c] 10,000 (Å^4)	−0.0002(2)	−0.0025(2)	0.0007(5)
Ni(2) $\frac{2}{3}\frac{1}{3}\frac{1}{4}$			
U_{11}[b] (Å^2)	0.0060(5)	0.0113(3)	0.0105(3)
U_{33}[b] (Å^2)	0.0077(5)	0.0112(3)	0.0102(3)
Occupancy	0.275(6)	0.524(4)	0.614(5)
Sn $\frac{1}{3}\frac{2}{3}\frac{1}{4}$			
U_{11}[b] (Å^2)	**0.0227(4)**	**0.0286(3)**	**0.0301(4)**
U_{33}[b] (Å^2)	0.0099(4)	0.0082(3)	0.0075(4)
C_{111}[c] 1000 (Å^3)	**−0.032(2)**	**−0.059(3)**	**−0.055(4)**
D_{1111}[c] 10,000 (Å^4)	**−0.009(2)**	**−0.053(3)**	**−0.052(2)**
D_{1133}[c] 10,000 (Å^4)	0.0002(3)	−0.0011(2)	−0.0005(3)
D_{3333}[c] 10000 (Å^4)	0.0002(3)	−0.0021(3)	−0.0002(3)
E_{11111}[c] 100,000 (Å^5)	**−0.029(3)**	**0.031(5)**	**0.104(9)**
E_{11133}[c] 100,000 (Å^5)	−0.0004(2)	−0.0016(3)	−0.0006(4)

The 'dominating' coefficients of the Gram-Charlier expansion of the pdf, i.e., those which modify the pdf mainly within the $a-b$ plane, are printed in bold. Trial refinements of the occupancies of the Ni(1) or Sn sites indicate no significant deviations from full occupation of these sites.

[a] In the course of the discussions the alloys compositions in italics are used to label the crystals.

[b] Gaussian anisotropic atomic displacement parameters within the 'harmonic approximation' according to the formula $T_{\mathrm{harm}}(hkl) = \exp[-2\pi^2 d^{-2}(U_{11}\cdot h^2 + U_{22}\cdot k^2 + \cdots + 2U_{23}kl)]$, where $T(hkl)$ is a factor with which the form factor of the corresponding atom has to be multiplied in the course of the calculation of the structure factor.

[c] Coefficients of a Gram-Charlier series expansion of the pdf to consider a non-Gaussian shape in three-dimensional space. Thus, the factor $T_{\mathrm{harm}}(hkl)$ is modified like $T_{\mathrm{GC}}(hkl) = T_{\mathrm{harm}}[1 + (2\pi i)^3 C_{mnp}h_m h_n h_p/3! + (2\pi i)^4 D_{mnpq}h_m h_n h_p h_q/4! + \cdots]$, where $h_1 = h$, $h_2 = k$ and $h_3 = l$.

the *Ni1.35Sn* crystal, for which a refined composition of only $Ni_{1.275}Sn$ is obtained. In order to analyze possible origins for these discrepancies the cell parameters of the alloys as determined by X-ray powder diffraction and the cell parameters determined from the selected single crystals are compared with known cell parameters vs. composition data ([5] and A. Leineweber, *unpublished*). For the *Ni1.35Sn* single crystal the refined Ni content is supported by the small cell parameters of that crystal (Fig. 2): If the cell volume data ($3^{1/2}/2a_{\mathrm{HT}}^2 c_{\mathrm{HT}}$ vs. δ) are linearly extrapolated to low Ni contents, the cell volume of the *Ni1.35Sn* crystal corresponds to $\delta = 0.28$. In contrast to the single crystal, a diffraction measurement from a powder made from the regulus gave a cell volume yielding $\delta = 0.38$ (cf. Fig. 2).

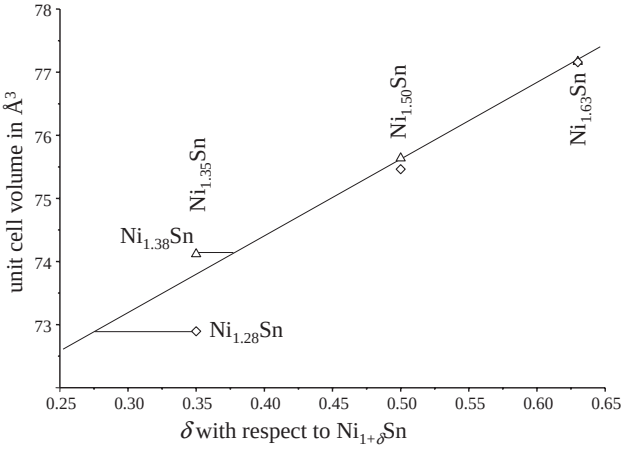

Fig. 2. Unit cell volumes, $3^{1/2}/2\cdot a_{\mathrm{HT}}^2\cdot c_{\mathrm{HT}}$, for HT-$Ni_{1+\delta}Sn$ as fitted to data from Ref. [5] compared with the results from powder (triangles) and single crystal diffraction experiments (diamonds) from the present alloys, for which the compositions from balancing ($Ni_{1.35}Sn$, $Ni_{1.50}Sn$ and $Ni_{1.63}Sn$) have been adopted for plotting. In particular, the *Ni1.35Sn* single crystal shows an unexpectedly small unit cell volume, which would correspond to a composition of $Ni_{1.28}Sn$. This is, however, consistent with the refined composition $Ni_{1.275(2)}Sn$ (cf. Table 3). The cell parameters of a powder sample prepared from a part of that alloy indicated a composition of $Ni_{1.38}Sn$.

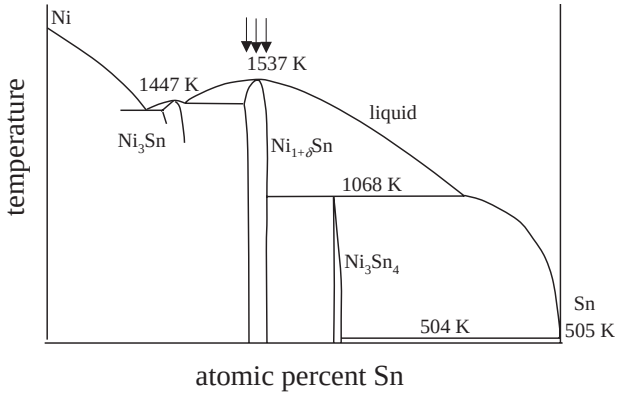

Fig. 3. Simplified phase diagram Ni–Sn after Ref. [7] explaining the constitutional origins of segregation and proposed origin of inhomogeneities in the $Ni_{1.35}Sn$ alloy. The three alloy compositions $Ni_{1.63}Sn$, $Ni_{1.50}Sn$ and $Ni_{1.35}Sn$ (in this sequence from the left to the right) are indicated by arrows.

The differences between the compositions of the powder prepared from the $Ni_{1.35}Sn$ alloy, the *Ni1.35Sn* single crystal and the value expected from weighting can be explained considering the phase diagram Ni–Sn [7] and, in particular, the low-nickel side of the $Ni_{1+\delta}Sn$ phase field (Fig. 3): The (HT-)$Ni_{1+\delta}Sn$ phase melts congruently at 1537 K and a composition of about $Ni_{1.50}Sn$. For low Ni contents the $Ni_{1+\delta}Sn$ phase coexists with the Ni-Sn liquid down to the peritectic temperature of Ni_3Sn_4. The Ni–Sn liquid has a degenerate eutectic at 504 K at a composition close to pure Sn ($T_{\mathrm{m}}(\mathrm{Sn}) = 505$ K). Therefore, an alloy of the

composition $Ni_{1.35}Sn$ is likely to show segregation upon solidification. This was in fact observed by optical micrographs using polarized light on polished cross sections (A. Leineweber, M. Ellner, E.J. Mittemeijer, *unpublished results*) of alloys cast into water-cooled copper molds which were used in the studies of Ref. [5]. For these alloys the segregation could be removed by homogenization with the heat treatment program also applied for the present alloys (cf. Section 2.1). However, the present alloys were solidified by relatively slow cooling (compared to solidification in the molds) in alumina crucibles. Therefore, even more severe segregation is expected than for casting into water-cooled molds. Furthermore, the present alloys have a larger grain size (about 1 mm) compared to 0.1 mm for $Ni_{1.35}Sn$ alloy cast in a mold. Consequently, it seems likely that the heat-treatment used in order to achieve homogenization was not fully successful for the $Ni_{1.35}Sn$ alloy, and that the selected crystal had—by accident—a considerably smaller Ni content than the average alloy's composition.

The Ni content $Ni_{1.275}Sn$ which was refined for the *$Ni_{1.35}Sn$* single crystal and which was supported by the cell parameters, is considerably smaller than allowed by the low-Ni side boundary of the $Ni_{1+\delta}Sn$ field. Below 1068 K the composition $Ni_{1.275}Sn$ should be located in a two-phase region $Ni_{\approx 1.35}Sn + Ni_3Sn_4$ (cf. Fig. 3 and Ref. [7]). In fact, recent experiments suggest that the $Ni_{1+\delta}Sn$ field extends to significantly lower Ni contents than $Ni_{1.35}Sn$ (A. Leineweber, *unpublished*).

3.2. Analysis of static displacements of Sn

An analysis of the Gaussian anisotropic atomic displacement parameters of the two Ni and the Sn sites indicates (Table 4) that except for the U_{11} values of Sn, the values U_{ii} (all U_{ii} values as listed in Table 3 correspond to the principal axis values due to site symmetry) range at about 0.01 Å^2 or below. This corresponds largely to the values obtained for long-range ordered LT′-/LT-$Ni_{1+\delta}Sn$ ($0.35 \leqslant \delta \leqslant 0.50$) by Rietveld refinement of powder diffraction data, where thermal contributions to the atomic displacement parameters should dominate [5]. The U_{11} parameters of Sn are considerably larger than all other U_{ii} values. Furthermore, only those coefficients of the Gram-Charlier expansion of the pdf of Sn, which modify the pdf within the $a-b$ plane (i.e., those, coefficients which contain only 1 and/or 2 in their index, but not 3) are considerably larger than the corresponding estimated standard deviation.

Although, starting from the ideal structure model of HT-$Ni_{1+\delta}Sn$ (Table 1 and Section 1), there should be least space for displacements of Sn within the $a-b$ plane, the observed strongly anisotropic and non-Gaussian atomic displacements are strongest within this plane. Therefore, these displacements are unlikely due to thermal vibrations of Sn in an anharmonic average potential. Instead, static displacements of Sn seem to be a probable explanation. It is expected that the occupation of the Ni(2) sites in the neighborhood of an individual Sn atom determines its actual position.

The dominant 'unusual' displacements of Sn can be made visible by Fourier sections showing the electron density of a section at $z = \frac{1}{4}$ containing the Sn and Ni(2) atoms (Fig. 4). For the *$Ni_{1.50}Sn$* and *$Ni_{1.63}Sn$* crystals a somewhat triangular shape of the electron density corresponding to the Sn atom is visible, with 'bulges' into the direction of the Ni(2) positions. This is less pronounced for the *$Ni_{1.35}Sn$* crystal.

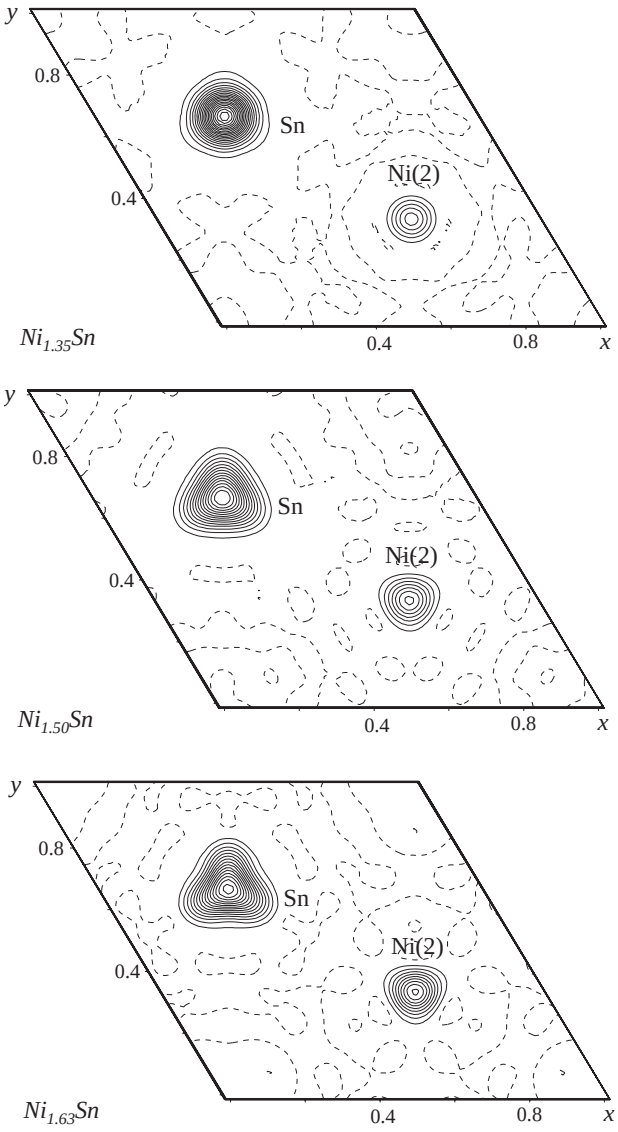

Fig. 4. Fourier sections indicating the electron density of the HT-phase unit for the three investigated crystals at $z = \frac{1}{4}$. The straight lines correspond to positive contours spaced by 20 e/Å^3, the dashed lines correspond to the zero-level.

Ideas about which local atomic arrangements may create the observed average electron densities in the HT-phase, can be obtained by inspecting the crystal structure of orthorhombic, ideally ordered LT-$Ni_{1.50}Sn$ (cf. Table 1 and Refs. [5,8]). A thorough discussion of the structural features of LT-$Ni_{1.50}Sn$ has been given in Ref. [5]. The most important points of this discussion will be outlined here as far as they are of relevance for the present considerations. The main feature of the LT-phase at $\delta = 0.50$ is the ordering of the Ni(2) atoms against the vacancies. This is reflected in a splitting of the Ni(2) sites of the HT-phase structure (occupied by Ni(2) and vacancies) into Ni(2a) and vacancies ('Ni(2b)') (cf. Table 1).

In the LT-phase the Ni(2a), Sn(a) and Sn(b) atoms are all located at $z = \frac{1}{4}, \frac{3}{4}$ (i.e., a mirror plane $\ldots/m$ in the space group symmetry *Pbnm*, $[001]_{LT} \| [001]_{HT}$). Sn(*a*) and Sn(*b*) are not only crystallographically inequivalent, but differ also 'chemically' by their different environments of closest Ni(2a) atoms: For Sn(a) the surrounding trigonal-bipyramid of five potential Ni(2) sites[1] is occupied in one equatorial (within the $a-b$ plane) and both axial (at $\Delta z = \pm\frac{1}{2}$) positions by Ni(2a) whereas two equatorial ones are empty. For Sn(b) only two equatorial positions are occupied by Ni(2a). Regarding further only the equatorial neighbors, i.e., in the same $a-b$ plane, one arrives at one Ni(2a) for Sn(a) and two Ni(2a) neighbors for Sn(b) (Fig. 5).

The different environments of Sn(a) and Sn(b) lead to different displacements of these Sn atoms from their 'ideal' positions (see Table 1): Sn(a) and Sn(b) are displaced by 0.173 and 0.293 Å, respectively, in different directions (Fig. 5). In contrast to Sn, the displacements of Ni(1) and Ni(2) in the LT-phase are considerably smaller.

The direction of the displacements of the Sn atoms was explained as follows [5]: Sn(a) is shifted in the direction away from its only Ni(2a) neighbor in the $a-b$ plane, and, therefore, the displacement direction is parallel to the equatorial direction Ni(2a)···Sn(a). The displacement direction of Sn(b) is parallel to the sum of the vectors connecting the two Ni(2a) neighbors with Sn(b). The different magnitude of the displacements of Sn(a) and Sn(b) can been made plausible with close contacts between the displaced Sn atoms and Ni(1) atoms: Simply said, there is more space in the direction into which Sn(b) is displaced. For more details cf. Ref. [5].

It is likely that also in the HT-phase $Ni_{1.50}Sn$ crystal Sn is coordinated within the $a-b$ plane mainly by either one or two Ni(2) atoms. Therefore, similar displacements of Sn should occur as in LT-$Ni_{1.50}Sn$. Fig. 6 shows how the displacements observed in the LT-phase should look like in HT-phase: There are three possibilities for both arranging one and two Ni(2) atoms

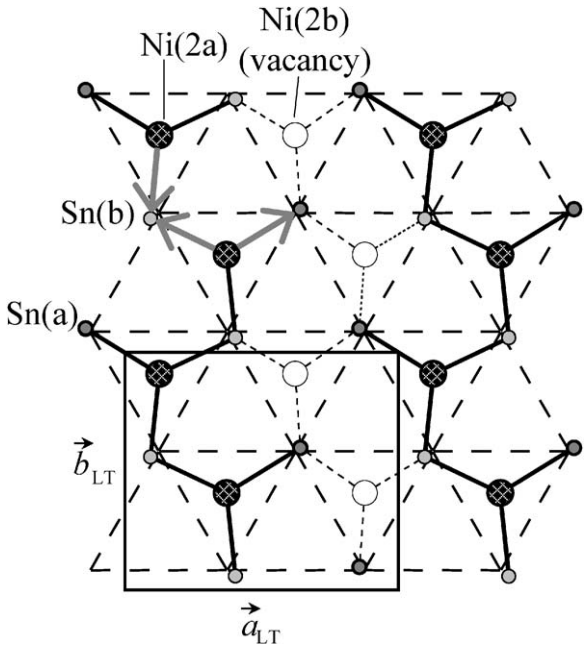

Fig. 5. Crystal structure of LT-$Ni_{1.50}Sn$: The atoms Ni(2*a*), Sn(*a*) and Sn(*b*) as well as the position of unoccupied trigonal-bipyramidal sites located at $z = \frac{1}{4}$ are shown. The gray arrows indicate the repulsive Ni(2a)···Sn interactions which determine the displacement directions of Sn(a) and Sn(b).

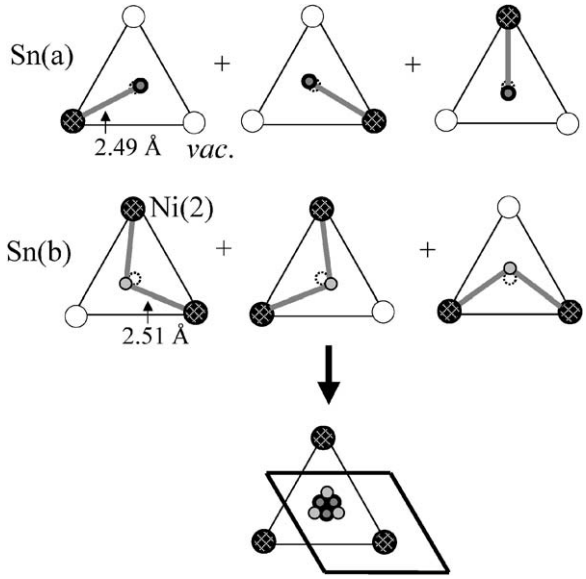

Fig. 6. Local configurations leading to the split atom model for HT-$Ni_{1.50}Sn$ on the basis of the different possible arrangements of Ni(2a) and vacancies (vac.) around Sn in LT-$Ni_{1.50}Sn$ (cf. Fig. 5). An equal probability of the six different configurations, three corresponding to Sn(a) and three to Sn(b), have the same probability of $\frac{1}{6}$. The ideal sites are indicated by dashed circles. The 'unit cells' are oriented like in Fig. 3.

[1] The trigonal-bipyramidal site on which partially Ni(2) is located is surrounded by a trigonal-pyramid of Sn atoms, but this holds also vice versa.

around a Sn atom, which leads to two different, threefold 'split atoms' called (as in the LT-phase) Sn(a) and Sn(b). The crystallographic description of these sites is (both on 6*h* Wyckoff site of $P6_3/mmc$, see Fig. 6):

Sn(a) x_a $2x_a$ $\frac{1}{4}$ with $x_a < \frac{1}{3}$,

Sn(b) x_b $2x_b$ $\frac{1}{4}$ with $x_b > \frac{1}{3}$.

Assuming like for LT-$Ni_{1.50}Sn$ a 1:1 occurrence of Sn(a) and Sn(b) in HT-$Ni_{1.50}Sn$, each of the above mentioned split site position would have an occupancy of $\frac{1}{6}$. On the basis of this *split atom model* a least-square refinement was performed on the single crystal X-ray diffraction data of the $Ni_{1.50}Sn$ crystal: Ni(1) and Ni(2) were considered as for the *main model*, Sn by the split atom description imposing the expected fixed occupancies of $\frac{1}{6}$ for both Sn(a) and Sn(b) and refined x_a and x_b parameters. One common isotropic atomic displacement parameter was refined for Sn(a) and Sn(b) in order to consider thermal displacements. The results of a refinement using the *split atom model* are listed in Table 5.

Very small improvements of residuals of the *split atom model* can be achieved by allowing for a refinement of the occupancies of the Sn(a) and Sn(b) sites, however, severe correlations between the displacement, positional and occupation parameters occur and the refinement becomes unstable. Therefore, such attempts were cancelled. Though, considering only either Sn(a) or Sn(b) sites leads to convergence, the agreement factors are considerably worse than with the two sites, i.e., using the complete *split atom model*.

Table 5
Results of an evaluation of the single crystal X-ray data obtained from the $Ni_{1.50}Sn$ crystal using the *split atom model*. $R(\mathrm{all}/I > 3\sigma(I)) = 0.0539/0.0303$, $R_w(\mathrm{all}/I > 3\sigma(I)) = 0.0705/0.0654$ (14 parameters)

Ni(1) 0 0 0	
U_{11} (Å^2)	0.0111(3)
U_{33} (Å^2)	0.0073(4)
D_{1111}[b] 10,000 (Å^4)	−0.010(1)
D_{1113}[b] 10,000 (Å^4)	0.0000(5)
D_{1133}[b] 10,000 (Å^4)	−0.0015(2)
D_{3333}[b] 10,000 (Å^4)	−0.0027(3)
Ni(2) $\frac{2}{3}\frac{1}{3}\frac{1}{4}$	
U_{11} (Å^2)	0.0131(3)
U_{33} (Å^2)	0.0123(3)
Occupancy of Ni(2)	0.523(4)
Sn(a,b) x, $2x$, $\frac{1}{4}$	
U_{iso} (Å^2)	0.0109(1)
x_a	0.3158(2)
Displacement of Sn(a) (Å)[a]	0.125(3) (0.173)
x_b	0.3711(1)
Displacement of Sn(b) (Å)[a]	0.268(2) (0.293)

[a] Distance of the $x_{a,b}$ $2x_{a,b}$ $\frac{1}{4}$ site from the ideal $\frac{1}{3}\frac{2}{3}\frac{1}{4}$ site. In brackets the corresponding distances as observed for the LT-phase [5] are given.
[b] See footnote c of Table 4.

The refinement of the *split atom model* gives reasonable residuals, which are only slightly worse than those of the *main model*. The occupancy of Ni(2) as well as the U_{ij} parameters of these models agree very well. Furthermore, the resulting U_{iso} value of Sn refined for the *split atom model* agrees well with the U_{11}/U_{33} components of the other atoms as well as the isotropic atomic displacement parameters observed for the LT/LT′-phases [5]. Therefore, it is reasonable to assume, that the refined U_{iso} value of Sn corresponds closely to the true dynamic contribution to the atomic displacements, whereas the static displacements are contained in the fractional coordinates of Sn(a) and Sn(b).

The fractional coordinates of the *split atom model* for Sn(a) and Sn(b) can now be used to calculate 'realistic' equatorial Ni(2)···Sn distances (see Fig. 6). One finds $d(\mathrm{Ni(2)\cdots Sn(a)})_{eq} = 2.493(1)$ Å and $d(\mathrm{Ni(2)\cdots Sn(b)})_{eq} = 2.514(1)$ Å, which are now of reasonable magnitude and similar to the values as observed for the LT-phase [5]. Relative to the ideal sites the Sn atoms ($\frac{1}{3}\frac{2}{3}\frac{1}{4}$) Sn(a) and Sn(b) are displaced by distances of 0.13 and 0.27 Å. These displacements in the HT-phase are somewhat smaller than the corresponding displacements in LT-$Ni_{1.50}Sn$ [5], which are 0.17 and 0.29 Å. This may partially be due to a less optimal local arrangement of the atoms in the HT-phase compared to the LT-phase. Furthermore, the present model considers only those local configurations which occur in the LT-phase, but e.g., for a purely statistical distribution of the Ni(2) atoms there should also be Sn atoms with only zero or three Ni(2) neighbors within the $a-b$ plane. Such Sn atoms should not—in a first approximation—be displaced at all within the $a-b$ plane.

The inspection of the structure of the LT-phase lead to the split atom description for the pdf for Sn. But by the same considerations also static displacements would be expected for Ni(1) and Ni(2). However, according to the structure of LT-$Ni_{1.50}Sn$ these displacements should be considerably smaller than for Sn(a) and Sn(b) [5]. The contributions from static displacements of Ni(1) and Ni(2) are, therefore, not easily separated from the thermal contribution and hidden in the refined atomic displacement parameters (U_{ij}, D_{mnqp}).

On the basis of the *split atom model* applied to the $Ni_{1.50}Sn$ crystal data, also the electron densities corresponding to Sn for the $Ni_{1.35}Sn$ and $Ni_{1.63}Sn$ crystals can be understood. For the $Ni_{1.63}Sn$ crystal the triangular shape of the electron density corresponding to Sn atom is somewhat more pronounced than for $Ni_{1.50}Sn$. On the basis of simple statistical considerations it can be shown that upon increasing the Ni content by increasing δ the Sn(b) atoms with two Ni(2) neighbors in the $a-b$ plane should become more frequent on cost of the occurrence of Sn(a) with only one Ni(2) neighbor. This

explains the observed tendency, since the more abundant Sn(b) atoms are just located at the 'bulges' of the electron density corresponding to Sn.

For the lower Ni contents ($Ni_{1.35}Sn$) the overall extent of the atomic displacements of Sn within the $a-b$ plane decreases. Furthermore, the electron density corresponding to Sn is closer to infinite rotational symmetry around [001]. This can be explained by a higher probability of Sn(a) and the effective absence of Sn(b). Therefore, the smaller displacements of Sn(a) become more dominant for the overall electron density.

In principle it is also possible to refine parameters of *split atom models* also for the $Ni_{1.35}Sn$ and $Ni_{1.63}Sn$ crystals. However, too severe instabilities and correlations occur for such refinements. This is mainly due to the fact that the occupancies of either Sn(a) (case of $Ni_{1.63}Sn$) or Sn(b) ($Ni_{1.35}Sn$) are expected to be very small. For sites with such small occupancies fractional coordinates cannot be refined. As for $Ni_{1.50}Sn$ simplified models with either only Sn(a) or Sn(b) do not give convincing results which can compete with the refinements using the *main model*. Therefore, no *split atom model* refinements for $Ni_{1.35}Sn$ and $Ni_{1.63}Sn$ are presented.

It has to be stated that the interpretation of the electron densities corresponding to Sn could only be done on the basis of certain perceptions concerning the displacements of Sn. Without the knowledge of expected atomic distances one could e.g., propose naively an alternative mechanism (cf. Fig. 7) which could lead to the same *split atom model* as given in Table 4: the displacements of Sn corresponding to Sn(a) are assumed to be caused by two and for Sn(b) by one neighboring Ni(2) atom, respectively. This would mean that in the six structures at the top of Fig. 6 the Ni(2) atoms and the vacancies would be exchanged, and the Ni(2) atoms would attract instead of repel the Sn atoms, which would give the situation shown in Fig. 7. The only criterion to discard the alternative mechanism are the expected unreasonably short Ni···Sn distances, however, not the present Bragg intensity data.

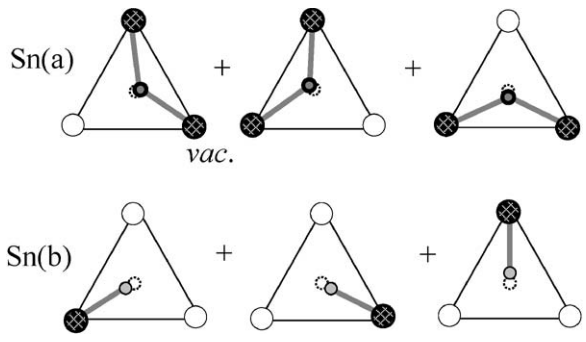

Fig. 7. Alternative model with other types of atomic displacements than in Fig. 6 leading to the same type of electron densities at the composition $Ni_{1.50}Sn$ (see text).

Experimentally, the problem the situations shown in Figs. 6 and 7 can be resolved considering the size-effect intensity transfer of diffuse scattering data on HT-$Ni_{1+\delta}Sn$ as observed previously by selected area electron diffraction [11]. The qualitative evaluation of the diffuse scattering suggested that the basal triangle of an Sn_5 trigonal-bipyramid around one Ni(2) is expanded, whereas it should be contracted for an empty trigonal-bipyramid. However, the qualitative interpretation of the diffuse scattering data only lead to the proposal that the Sn atoms would be displaced like Sn(*a*). The 'interaction' between the displacements by two Ni(2) on one Sn leading to Sn(b) with a different displacement direction as compared to Sn(a) was not considered explicitly and is probably difficult to be deduced in the course of a qualitative evaluation of diffuse scattering. In order to derive this, the present evaluation of the Bragg intensity data was very successful and straightforward.

The results concerning $Ni_{1.63}Sn$ are qualitatively comparable to what has been observed previously for $Fe_{1.60}Ge$ [12] and $Fe_{1.67}Ge$ [13], where a split atom model based on a single Ge(b) site (according to the presently used nomenclature) was used to describe the static displacements of Ge. However, the studies on $Fe_{1+\delta}Ge$ were restricted to a narrow range of compositions in the system Fe-Ge, whereas now a wide range of composition was studied, revealing the static displacements into different directions corresponding to Sn(a) *and* Sn(b).

The structural features observed here for HT-$Ni_{1+\delta}Sn$ (and previously on $Fe_{1+\delta}Ge$) of Ni_2In/NiAs type structure are probably also present in other disordered phases having this structure type and an intermediate value of δ (neither 0 nor 1). However, in literature there is an apparent lack of detailed structural studies of such disordered phases except for $Fe_{1+\delta}Ge$. Such phases with their apparently simple crystal structure were often only characterized by indexed powder diffraction patterns without a quantitative evaluation of reflection intensities. More thorough diffraction investigations on such disordered phases should clarify this situation. However, instead of obtaining more detailed information about an alleged disordered phase, it can also turn out that this phase shows in fact long-range order, as revealed previously for some cases when e.g., selected area electron diffraction was applied [20].

4. Conclusions

(i) The crystal structure of HT-$Ni_{1+\delta}Sn$ was studied by X-ray diffraction on three different crystals $Ni_{1.35}Sn$, $Ni_{1.50}Sn$ and $Ni_{1.63}Sn$ (the alloys had these average compositions) which have the refined compositions of $\delta = 0.275$, 0.524, 0.614. The

previously reported Ni_2In/NiAs structure type ($P6_3/mmc$) with Ni(1): 2*a*, 0 0 0, Ni(2), 2*d*, $\frac{2}{3}\frac{1}{3}\frac{1}{4}$, occupancy δ, and Sn: 2*c*, $\frac{1}{3}\frac{2}{3}\frac{1}{4}$ is basically confirmed. However, the electron density based on refinement of atomic displacement parameters revealed an electron density of Sn, which is strongly extended within the $a-b$ plane. This feature varies significantly with composition: These displacements are most exhibited for $Ni_{1.63}Sn$, least for $Ni_{1.35}Sn$.

(ii) The displacements of Sn can be understood—based on the crystal structure of the ordered low-temperature phase LT-$Ni_{1.50}Sn$—as resulting from a superposition of different local atomic configurations, i.e., different number of Ni(2) atoms (mainly one or two) around one Sn in the $a-b$ plane, leading to different amounts and directions for static displacements of Sn. The magnitude of the displacements in the HT-phase (data from $Ni_{1.50}Sn$) from its ideal position $\frac{1}{3}\frac{2}{3}\frac{1}{4}$ is somewhat smaller than observed for LT-$Ni_{1.50}Sn$, but shows good qualitative agreement.

(iii) The presence of the large static displacements for Sn confirms that the simple average fractional coordinates for Ni(1), Ni(2) and Sn (see (i) and Table 1) in the HT-phase must not be used to calculate interatomic distances, in particular not for Ni(2)⋯Sn within the $a-b$ plane, which would be unrealistically small. This should in general be considered for atomic distance calculations on the basis of fractional coordinates obtained of a not fully ordered crystal structure, if the presence of considerable static displacements cannot be excluded.

Acknowledgments

Prof. Dr. E.J. Mittemeijer (Max Planck Institute for Metals Research, Stuttgart, D) first suggested the presence of static displacements in $Ni_{1+\delta}Sn$. A.L. thanks him for his support and interest in the work, and Dr. Václav Petříček (Praha, CZ) for his help in the use Jana2000 and for many recent modifications of this program.

Further details of the crystal structure investigation(s) on the $Ni_{1.50}Sn$ single crystal (*split atom model*) can be obtained from the Fachinformationszentrum Karlsruhe, 76344 Eggenstein-Leopoldshafen, Germany, (fax: +49-7247-808-666; crysdata@fiz.karlsruhe.de) on quoting the depository number CSD 391238.

References

[1] M.A. Krivoglaz, Diffraction of X-rays and Thermal Neutrons in Imperfect Crystals, Springer, Berlin, 1992.
[2] W.F. Kuhs, Aust. J. Phys. 41 (1988) 369.
[3] J.-M. Joubert, R. Černý, M. Latroche, E. Leroy, L. Guénée, A. Percheron-Guégan, K. Yvon, J. Solid State Chem. 166 (2002) 1.
[4] A. Leineweber, M. Ellner, E.J. Mittemeijer, J. Solid State Chem. 159 (2001) 191.
[5] A. Leineweber, J. Solid State Chem., in press.
[6] A. Leineweber, E.J. Mittemeijer, M. Knapp, C. Baehtz, Mater. Sci. Forum 443–444 (2004) 247.
[7] P. Nash, A. Nash, Bull. Alloy Phase Diagr. 6 (1985) 350.
[8] P. Brand, Z. Anorg. Allg. Chem. 353 (1967) 270.
[9] L.P. Komarovskaya, L.G. Aksel'rud, R.V. Skolozdra, Kristallografiya 28 (1983) 1201.
[10] P. Brand, Z. Anorg. Allg. Chem. 358 (1968) 170.
[11] A.-K. Larsson, R.L. Withers, L. Stenberg, J. Solid State Chem. 127 (1996) 222.
[12] B. Malaman, J. Steinmetz, B. Roques, J. Alloys Compd. 75 (1980) 155.
[13] F. Albertini, L. Pareti, A. Deriu, D. Negri, G. Calestani, O. Moze, S.J. Kennedy, R. Sonntag, J. Appl. Phys. 84 (1998) 401.
[14] B.H. Toby, CMPR—package of programmes, National Institute of Standards, 2000; http://www.ncnr.nist.gov/xtal
[15] K. Koths, ASIN, Version 7.4, 1987 (based on a code by F. Stewner, 1970).
[16] M. Dušek, V. Petříček, M. Wunschel, R.E. Dinnebier, S. van Smaalen, J. Appl. Crystallogr. 34 (2001) 398.
[17] W. Herrendorf, Habitus, University of Karlsruhe, 1993.
[18] A.J.C. Wilson, Intern. Tables Crystallogr. Vol. C., Kluwer Academic Publishers, Dordrecht, 1992.
[19] P.J. Becker, P. Coppens, Acta Crystallogr. A 30 (1974) 129.
[20] S. Lidin, A.-K. Larsson, J. Solid State Chem. 118 (1995) 313.